

Coupling of Thermal and Electrical Systems for the Simulation of ECS Architectures

Nicolás Ablanque Mejía¹ Sriram Karthik Gurumurthy² Santiago Torras Ortiz¹ Antonello Monti²
Joaquim Rigola¹ Carles Oliet¹

¹Universitat Politècnica de Catalunya - Barcelona Tech (UPC), Heat and Mass Transfer Technological Center (CTTC), Spain, {nicolas.ablanque, santiago.torras, joaquim.rigola, carles.oliet}@upc.edu

²ACS, EONERC, RWTH Aachen University, Germany, {sgurumurthy, amonti}@eonerc.rwth-aachen.de

Abstract

This work is focused on the coupling of two complex models based on different underlying physics: a vapor compression refrigerating system and its electrical drive system. The main challenge was to correctly handle the large simulation time constant difference which is three orders of magnitude smaller for the electrical system. The two models have been originally developed following very specific requirements (i.e. high numerical robustness and low time consumption) for their suitable use in simulations of large and complex aircraft Environmental Control Systems (ECS). The direct coupling of both systems has been observed to cause numerical instabilities, therefore, a coupling approach based on non-invasive dynamic relaxations has been implemented. The resulting combined simulations have shown to be numerically stable for the complete range of operating conditions and for a wide range of time steps.

Keywords: Multi-physics, Vapor compression system, Electrical drive system, Systems coupling

1 Introduction

The aviation industry has witnessed significant advancements in recent decades, supported by remarkable innovations. While aviation has made substantial contributions to society, certain critical issues resulting from the growth of commercial air travel need attention. The foremost concern is its impact on climate change, primarily due to the release of CO₂ emissions. To tackle these challenges, the industry has embraced a strategy that involves replacing mechanical, hydraulic, and pneumatic systems with electrically driven systems. This shift has given rise to the term "More Electric Aircraft" (MEA) within the industry (Sarlioglu and Morris 2015). The ECS is responsible for maintaining cabin temperature and pressure. It traditionally uses the bleed air from the main engines for its operation. However, under the MEA paradigm, the ECS has undergone a transition to be electrically fed (Sarlioglu and Morris 2015).

The novel ECS architectures within the MEA framework may include a Vapor Compression System (VCS) powered by an electrical motor drive with the aim to

provide higher efficiency additional cooling power to the cabin. In this paper, the combined simulation of the two aforementioned systems is addressed. On the one hand, the VCS system consists of a single-stage compression configuration including a centrifugal compressor, an air-to-refrigerant condenser (to eject heat into the aircraft ram air ducts), and a refrigerant-to-liquid evaporator (to indirectly extract heat from the cabin). This VCS provides additional cooling power to the cabin. It can be turned on and off during the flight according to the cabin cooling needs. The model developed to simulate the VCS system has been introduced in a previous work (Ablanque et al. 2023). On the other hand, the electrical system consists of a three phase inverter which drives a Permanent Magnet Synchronous Motor (PMSM). The Field Oriented Control strategy (FOC) has been adopted for the control of the PMSM drive (Irwin 1997). The PMSM drive is equipped with speed and torque control. The speed requested by the VCS is delivered by the electrical system.

In this paper, the goal is to successfully couple the thermal and electrical systems and conduct numerous simulation tests to validate the correct operation of the system. Discussions about the coupling strategy of two systems, the time steps adapted for the simulations and the results of the simulations are provided. Since the angular speed of the PMSM and VCS are different, the shafts of the two system are coupled through a gear box. The two systems are based on different domains of physical laws and ideally require different time steps for optimal simulation. The electrical system typically requires very small time steps for Electro-Magnetic Transient (EMT) simulations (in the range of 1 to 100 μ s) while the VCS time step is significantly larger (about 1 second). The electrical system is modelled in the dynamic phasor domain instead of EMT domain for increasing the time step to the range of 1 second such that it is compatible with the VCS system (Gurumurthy et al. 2022; Loka et al. 2022; Demiray 2008). To avoid non-smooth changes of torque from the VCS side and non-smooth changes of speed from the electrical side, a non-invasive dynamic relaxation strategy has been introduced. The dynamics of the individual thermal or electrical models are not internally modified with this approach. It consists in numerically relaxing the torque

and speed values exchanged across the mechanical flanges of the two systems. The coupled VCS-PMSM drive system is tested for various scenarios such as initial switch-on of the system, various speed reference changes, and more importantly, the starting-up and switching-off of the two systems while the simulation is being conducted. This paper also analyzes the computation CPU time of the model for various time steps to show the computational effectiveness of the proposed thermal-electrical system.

The paper is organized as follows: Section 2 describes the VCS and its testing procedures, followed by numerical simulation results of the VCS. The electrical system description, testing procedure and numerical simulation results are carried out in Section 3. The coupling strategy of the thermal-electrical system, the multi-physics simulation results, and the computational burden evaluation of the coupled simulations are carried out in Section 4. Finally, the conclusions and future work are presented in Section 5.

2 Vapor Compression System Model

2.1 Description

The vapour compression system model represents a typical single-stage configuration with four fundamental components: a centrifugal compressor, a refrigerant-to-air condenser, an expansion device, and a refrigerant-to-liquid evaporator. Additional minor components are also considered in the model such as connecting pipes, a reservoir, a by-pass valve and a super-heating sensor. Figure 1 shows the model internal scheme.

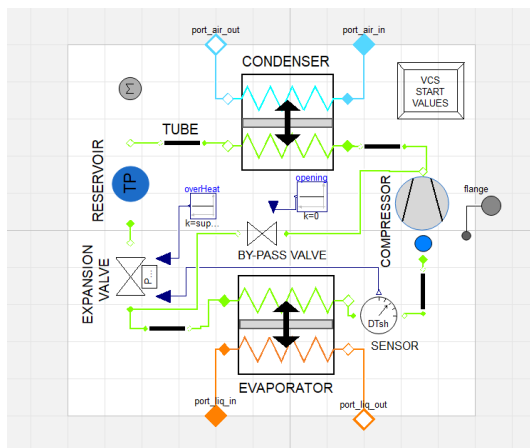


Figure 1. Vapor compression system scheme.

The vapor compression system model has been developed for its use within large thermal-electrical architectures of aircraft environmental systems. It must be thermally and electrically coupled to other subsystems. More specifically, the condenser exchanges heat with a ram air circuit (through inlet and outlet air fluid connections), the evaporator exchanges heat with a liquid circuit (through inlet and outlet liquid fluid connections), and the compressor exchanges mechanical variables with the electric drive

system (through a single mechanical connection).

2.2 Numerical Assessment and Tests

To successfully conduct simulations at the architecture level is particularly challenging due to many reasons such as the high number of components being solved, the high number of interactions between systems, the different physics being considered, and the necessity of low computing time consumption. Therefore, to prevent resolution issues, the vapor compression system model has been developed to fulfill demanding numerical robustness requirements and has been subjected to comprehensive series of tests focused on achieving the following aspects:

- The model must initialize correctly independently of the boundary condition values (the values at the boundary conditions are shared with other systems and they can vary dramatically during the initialization calculations).
- The model must be correctly simulated independently of the main simulation set-up parameters such as the stop time and the interval length (the set-up is common to all architecture systems).
- The model must be robust for all possible combinations of fluid boundary types. The fluid connections can be defined from the pressure values at both ends (P-P), or alternatively, from the pressure and the mass flow rate values at opposite ends (M-P). The model must also handle different input signal types for the boundary condition variables such as constant, step, ramp or sine.
- The vapor compression system model must be able to be turned on and/or off as many times as necessary and at any moments of the architecture simulation. In such cases, the simulation of the other systems involved should continue without being affected.
- The CPU time needed for the model to simulate dynamic and steady-state cases must be relatively low to prevent numerical bottlenecks at the architecture level (the maximum time required for steady-state simulations has been set at 10 seconds).

2.2.1 Initialization and steady-state tests

A complete set of runs has been generated to test the model robustness during initialization and the corresponding resolution time for steady-state conditions. The dataset has been built-up taking into account different values for all the boundary conditions (i.e. compressor speed, air and liquid temperatures, air and liquid mass flow rates, and air pressure) covering the whole physical range of possibilities and all its possible combinations. In addition, different fluid boundary condition types (see Figure 2) and different values for the interval length were also taken into consideration.

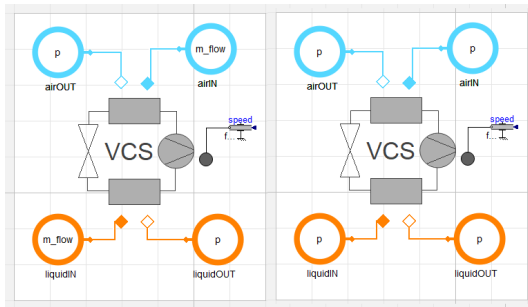


Figure 2. Boundary condition types: M-P (left) and P-P (right)

The tested runs consisted of 5400 cases (900 cases for each combination of boundary condition type and interval length). The simulation stop time was set at 2000 seconds so that the steady-state condition can be reached before. The main statistics obtained from the model simulations are summarized in Table 1.

Table 1. Initialization and steady-state convergence of VCS model: main statistics

Boundary type	Interval length	Mean CPU time	Failure rate type
	[s]	[s]	[%]
M-P	4	1.40	0
M-P	2	1.58	0
M-P	1	1.86	0
P-P	4	1.42	0
P-P	2	1.59	0
P-P	1	1.88	0

The results have shown that the model initialization is successful for all the cases without being affected by the interval lengths used or the combination of boundary values. The mean simulation time calculated for all cases is 1.6 seconds which is well below the threshold of 10 seconds required (in fact no cases were found to have a simulation time above 10 seconds).

2.2.2 Start-up and shut-down tests

A complete set of cases has also been generated to test the model robustness during shut-down and start-up demanding transients. These cases are mostly based on the same combinations and characteristics defined in the previous section. However, instead of reaching a steady-state condition, the system is now subjected to consecutive shut-downs and start-ups every 1000 seconds (the stop time for simulations is now 5000 seconds).

In this case, the whole set of cases has also been successfully simulated without experiencing any numerical issue. Illustrative results for a particular case are shown in Figure 3 in terms of the VCS refrigerant mass flow rate and the CPU time consumption (the mass flow rate is presented in dimensionless form due to confidentiality reasons). It can be observed from the CPU time evolution that the solver requires additional efforts during the main

dynamic events.

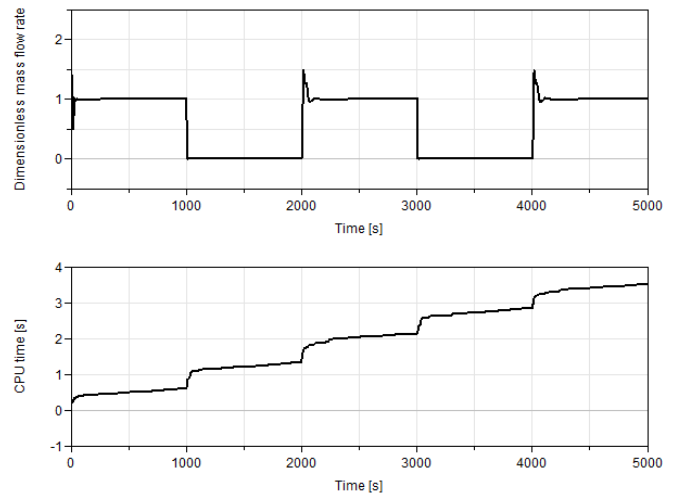


Figure 3. VCS model refrigerant mass flow rate and CPU time consumption during start-up shut-down test

2.2.3 Additional transient tests

Finally, it is worth mentioning that the model has been subjected to additional tests to ensure its robustness for different dynamic changes of the boundary condition variables based on the input signal type as shown in Figure 4 for the step and sine cases.

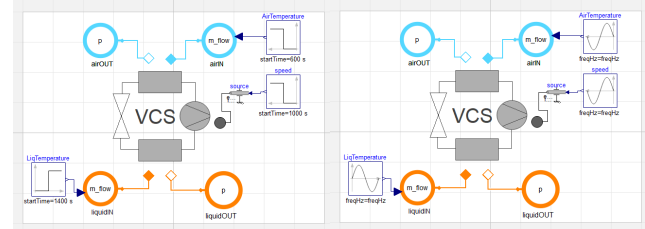


Figure 4. Boundary variable signal types: step (left) and sine (right)

The whole data-set prepared to test signals has also been successfully simulated by the model. Illustrative results for a particular case with sine signals are presented in Figure 5 in terms of the VCS compressor suction and discharge dimensionless pressures.

3 Electrical Drive System

3.1 Description

The model of the electrical system considered is shown in Figure 6. The system consists of a three-phase 2-level converter that interfaces a DC power supply and a permanent magnet synchronous motor (PMSM). The motor controller is equipped with field oriented control to track the reference speed supplied to motor controller. The motor controller achieves speed reference tracking by actively controlling the output voltage vectors of the three-phase inverter. The electrical drive system would be coupled

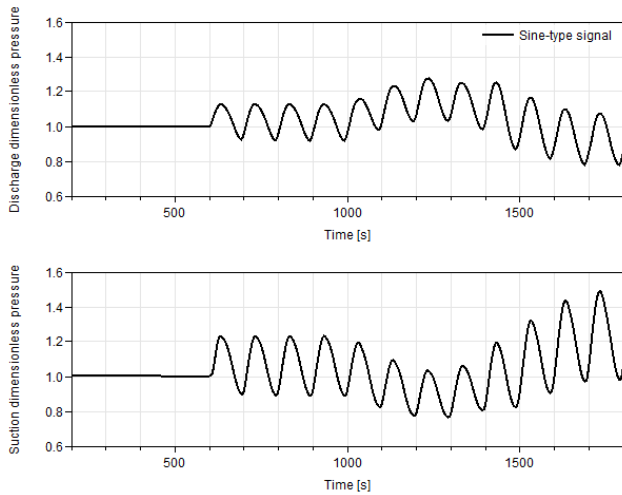


Figure 5. VCS suction and discharge pressures under transient conditions (sine signal)

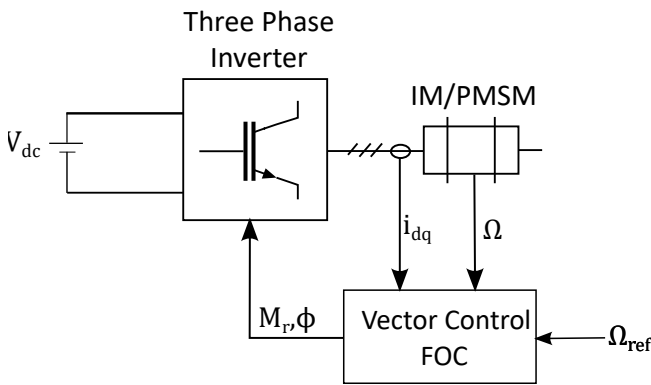


Figure 6. Electrical drive system

with the VCS system and therefore the electrical model needs to be robust and stable when load torque changes and speed changes occur. A short description of the electrical drive system is provided followed by detail simulation results to test the electrical motor.

3.1.1 PMSM

The PMSM is modelled in the dynamic phasor domain similar to (Irwin 1997; Loka et al. 2022). The flux in the stator λ_{ps} depends only on the stator currents i_{ps} since there is no electrical circuit in the rotor (Irwin 1997; Krause et al. 2013). The stator flux real part depends on the permanent magnet flux λ_f from the rotor as shown in Eq. (1).

$$\begin{bmatrix} \lambda_{ps,re} \\ \lambda_{ps,im} \end{bmatrix} = \begin{bmatrix} L_{sd} & 0 \\ 0 & L_{sq} \end{bmatrix} \begin{bmatrix} i_{ps,re} \\ i_{ps,im} \end{bmatrix} + \begin{bmatrix} \lambda_f \\ 0 \end{bmatrix} \quad (1)$$

L_{sd} and L_{sq} represent the direct and quadrature axis self-inductance. The stator currents are controlled by the applied stator voltage v_{ps} and electrical supply angular frequency ω_s of the three phase inverter as shown in (2).

$$\frac{d\lambda_{ps}}{dt} = v_{ps} - r_s i_{ps} - j\omega_s \lambda_{ps} \quad (2)$$

The electrical torque T_e developed by the PMSM is given by (3). The differential equation corresponding to the mechanical angular speed of the motor Ω_m is given by (4) where T_L is the load torque applied on the motor from the coupled external system, B is the coefficient of rotational friction, J is the inertia of the PMSM.

$$T_e = \frac{3}{2} p (\lambda_f i_{ps,im} + \Delta L \cdot i_{ps,re} i_{ps,im}) \quad (3)$$

$$J \frac{d\Omega_m}{dt} = T_e - B\Omega_m - T_L \quad (4)$$

The PMSM model is included to have the electrical loss, mechanical loss and efficiency calculations.

The PMSM is controlled through field oriented control (FOC). The controller consists of three levels, the outer level is a speed controller modelled by a PI controller. The speed controller synthesizes the torque reference. By Maximum Torque per Ampere (MTPA) strategy (Irwin 1997), the reference currents are calculated. An inner current controller tracks the stator current of the PMSM by actively controlling the output voltage vectors of the inverter.

3.1.2 Three phase inverter

We consider a 2-level inverter with B6C topology for the three-phase inverter. Harmonics introduced by the three phase inverter are neglected and the three-phase inverter is modelled as a fundamental phasor. A model that considers switching harmonics can be found in (Gurumurthy et al. 2022; Holmes and Lipo 2003; Ruan et al. 2018). The dynamic phasor of the phase to neutral voltage of phase A v_{an} is given by (5).

$$\langle v_{an} \rangle_0 = \frac{M_r V_{dc}}{4} e^{j\varphi} \quad (5)$$

The voltage on the DC link is V_{dc} and the control variables are Modulation ratio M_r and phase-shift angle φ . The conduction and switching loss evaluation of the power electronic switches are performed and these calculations are included within the model (Loka et al. 2022; Bierhoff and Fuchs 2004; Acquaviva et al. 2020).

3.2 Numerical testing and simulation results

To test the numerical robustness of the PMSM drive model, several tests are conducted. The drive model needs to control the speed of the motor adhering to the speed reference command provided by the VCS system. The speed reference needs to be maintained while supplying the required load torque and power that the VCS system requires. Furthermore, when the speed reference is increased, the torque required by the VCS system also increases. This adds further dynamic constraints that needs to be taken care by the motor controller.

The following tests are proposed to validate the drive operation. Notice that the speed and torque values are referred to the electrical motor side and not to the VCS side.

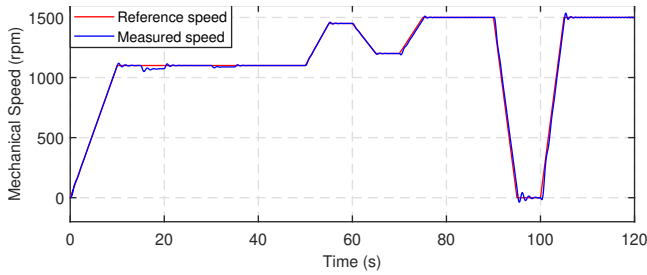


Figure 7. Comparison of reference speed and actual motor speed

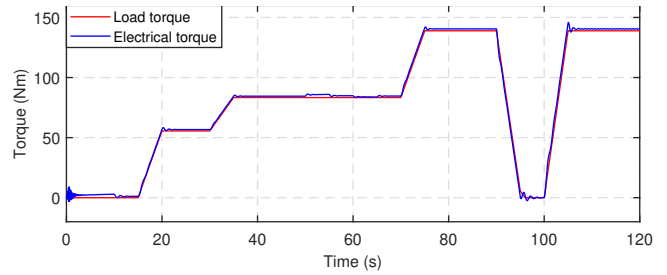


Figure 8. Comparison of applied load torque and electrical torque produced by PMSM

A specific gear ratio value had to be considered for the conversion of speed and torque values to the VCS side.

- At $t = 0s$ to $t = 10s$, the motor is switched-on and accelerated to a speed reference of 1100 rpm with torque 0 Nm.
- At $t = 15s$ to $t = 20s$, the torque is increased linearly to 55.5 Nm while the motor tries to maintain the speed.
- At $t = 30s$ to $t = 35s$, the torque is increased linearly to 83.3 Nm while the motor tries to maintain the speed.
- At $t = 50s$ to $t = 55s$, the motor is accelerated to a speed reference of 1450 rpm.
- At $t = 60s$ to $t = 65s$, the motor is decelerated to a speed reference of 1200 rpm.
- At $t = 70s$ to $t = 75s$, the motor is accelerated to a speed reference of 1500 rpm and simultaneously, the torque is also linearly increased to 139 Nm.
- At $t = 90s$ to $t = 95s$, the motor is controlled to speed reference 0 rpm and 0 Nm torque to validate a stand-still behavior.
- At $t = 100s$ to $t = 105s$, the motor is controlled to speed reference 1500 rpm and 139 Nm torque to validate the recovery from stand-still position.

Fig. 7 shows the comparison of reference speed and the actual motor speed. The start-up of the motor is smooth without oscillations and the speed reference changes are also accurately tracked without oscillations and steady state error.

During sudden load torque changes at $t = 15s$ and $t = 30s$, the speed does not change drastically due to fast torque control action as shown in Fig. 8. It can be observed that the electrical torque is greater than the mechanical load torque due to frictional losses.

The power losses occurring in the PMSM are shown in Fig. 9, which are consisting of electrical losses and mechanical losses. The electrical losses are dependent on the operating currents which in-turn depend on the required

torque. The mechanical frictional losses mainly depends on the operational speed of the motor. The overall peak efficiency of the PMSM is approximately 98 %.

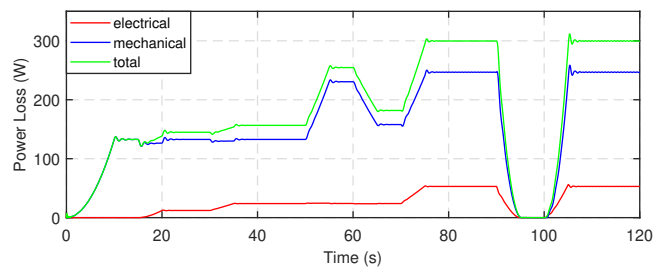


Figure 9. Power losses in the PMSM

The inverter losses consists of switching losses and conduction losses occurring in the IGBTs and the diodes. The inverter losses are shown in Fig. 10. The conduction and switching losses are functions of operational currents and voltage which are mainly dependent on the operational torque of the motor. The three phase inverter peak efficiency is approximately 97.5 %.

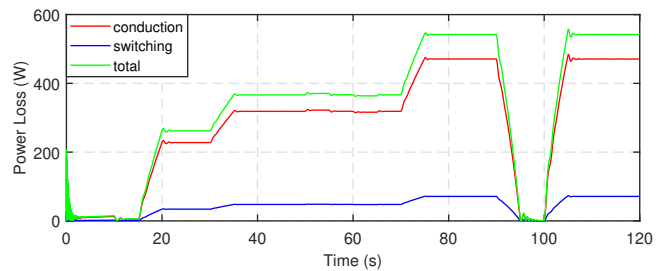


Figure 10. Power losses in the three phase inverter

4 Coupling of Thermal and Electrical Systems

4.1 Description

The VCS model has been coupled with the electrical drive system as shown in Figure 11. The VCS is based on fluid-dynamic and thermal physics while the drive system is based on electric physics. The latter system is aimed to power the compressor and to regulate its speed based on

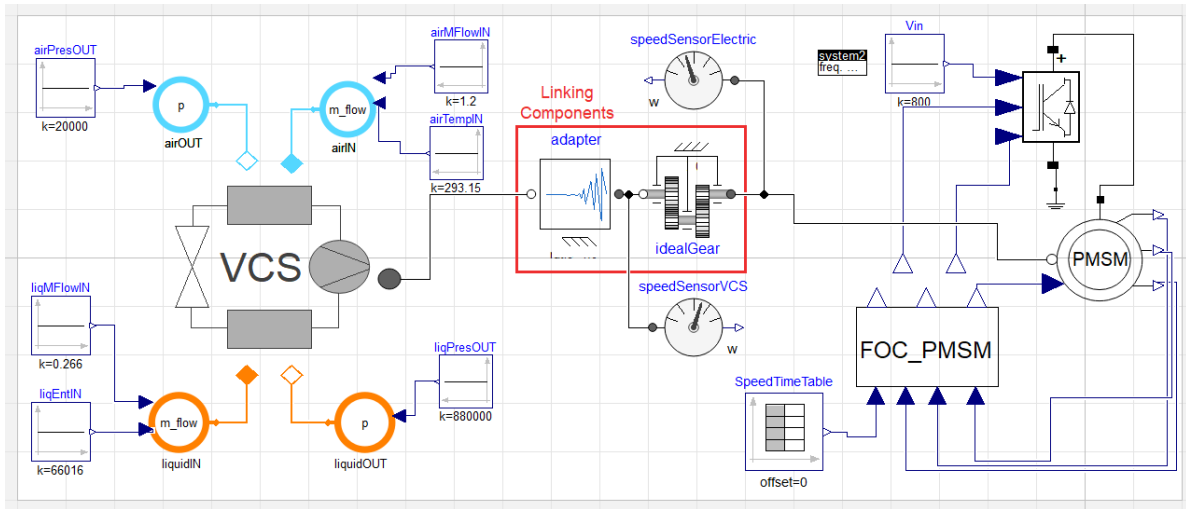


Figure 11. VCS and electrical drive system coupling scheme

an input signal provided by an external control mechanism (for the present tests the signal has been provided by appropriate source blocks). The two systems are mechanically linked so that the compressor rotating shaft parameters, namely, torque and speed, are shared by the two systems.

Two additional elements have been added to the mechanical linking. Firstly, an ideal gear component from the Modelica Standard Library has been used to match the operating characteristics of both systems. And secondly, due to uncontrolled oscillations observed when direct mechanical coupling was conducted, an additional non-invasive component integrating dynamic relaxation equations has been added. This component acts as a numerical hinge for the solver to avoid unstable numerical iterations when steep changes are experienced by both shared values: the torque and the speed. The aforementioned connecting element reduces the torque that the electrical system receives, and similarly, it moderates the speed that the compressor of the thermal system receives. In this way, rapid changes, such as start-ups or shut-downs are dampened, and the resolution does not collapse. The equations used are as follows:

$$\frac{d\phi}{dt} = \frac{(\phi_{aux} - \phi)}{\alpha_{\phi}} \quad (6)$$

$$\frac{d\tau}{dt} = \frac{(\tau_{aux} - \tau)}{\alpha_{\tau}} \quad (7)$$

Where ϕ and τ are the rotation angle and the torque in the coupling shaft, respectively. The time constant for relaxation, α , is used to avoid numerical instabilities and can be modified by the user.

4.2 Simulation

4.2.1 Expected performance

The simulations have been conducted in order to test the system capability and to achieve the following character-

istics:

- Robustness during the initialization (i.e. resolution at time step zero) which is usually a critical numerical aspect for the solver due to unknown values of the variables at the previous time step.
- Ability to conduct simulations at different fixed time steps (i.e. interval length defined in the simulation set-up). This characteristic is also crucial as the two systems studied herein are intended to be simulated together with all the other thermal and electrical systems of the complete ECS architecture.
- Robustness to handle start-up and complete switch-down conditions during the simulations. This numerically challenging feature is necessary due to the intermittent use of the VCS within the ECS operation.
- Low CPU resolution time to reduce the impact on the time consumption for the whole ECS simulation. This will allow real time based simulations and also to carry out simulations of large data-sets for design, prediction and/or control studies.

4.2.2 Results

The simulation baseline case to test all the aforementioned requirements is described as follows: an initial start-up procedure (time = 0 s), followed by a rapid complete shut-down of the system (at time = 500 s), then a rapid start-up again (at 1500 s), and finishing at stop time of 3000 s. The solver used for all cases was the default integration method DASSL.

Figure 12 shows the compressor rotating speed evolution for the baseline case dynamic simulation. The figure shows both the compressor speed value for the VCS and the rotational speed value provided by the electrical drive in order to see the impact of the mechanical relaxation applied to the systems coupling. Similarly, Figure

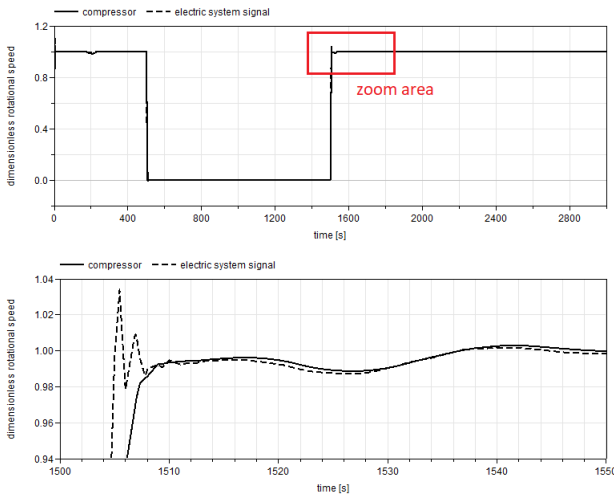


Figure 12. Rotational speed evolution. Top: whole simulation period. Bottom: zoom area in a start-up event

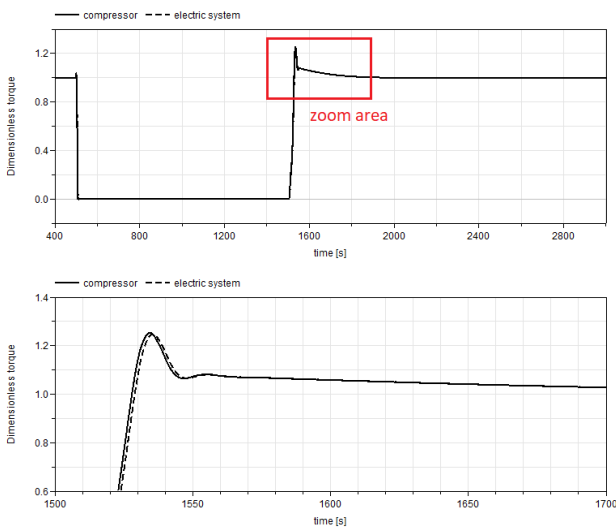


Figure 13. Torque evolution. Top: whole simulation period. Bottom: zoom area in a start-up event

13 shows the compressor torque evolution. The values of both shared variables, namely, the rotational speed and the torque, are practically the same for both systems during the whole simulation except for the moment of fast dynamic changes. The dynamic relaxations applied at the mechanical coupling have proven to provide numerical robustness for such transitions with a minimum cost (the discrepancies observed at such critical moments are not significant for the global result).

The baseline case has been simulated considering different values for the time step (i.e. interval length of the simulation set-up) to evaluate its numerical robustness but also its computational time consumption. The results are summarized in Table 2. The results show very good performance in terms of real time factor for all cases ($RTF = CPUtime/realtime$) and also, as expected, important resolution time differences between the time step

values considered.

Table 2. Time consumption and time step assessment

Time step [s]	CPU time [s]	real time factor
5	26.4	0.0088
1 ^a	24.9	0.0083
0.5	30.7	0.0102
0.1	51.2	0.0170
0.05	69.3	0.0231
0.01	99.3	0.0331
0.005	171.9	0.0573
0.002 ^b	349.7	0.1165

^aTypical value for VCS, ^b typical value for electrical drive

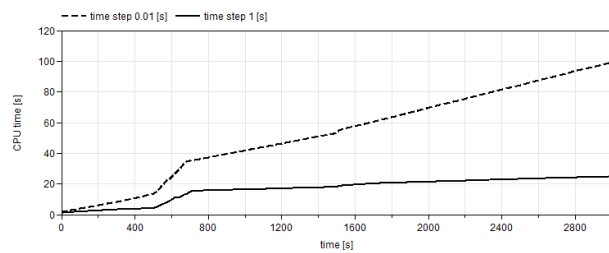


Figure 14. CPU time evolution for two different time steps

Finally, Figure14 shows the CPU time consumption evolution for two representative cases with different time steps. This Figure allows to see the solver stress level at different moments. In this sense, based on the CPU time slope, we can observe that the shut-down procedure and the transition to the off condition are more stressful for the solver than the start-up procedure.

5 Conclusions

The present work dealt with the linking of two models based different underlying physics: a vapor compression system and its electrical drive. The linking has been conducted using mechanical components to represent the compressor shaft.

- Both models have been independently tested to ensure appropriate numerical performance in terms of robustness and CPU time consumption.
- The combined simulation of the resulting thermal-mechanical-electrical model has been assisted with dynamic relaxations for the applied to the mechanical linking parameters, namely, rotational speed and torque.
- The combined model has proven to be numerically robust at critical conditions (initialization, start-up and shut-down procedures), independently of the simulation set-up configuration, and with low time consumption (adequate to simulate large data-sets of cases and real time calculations).

- The combined model is suitable for integrated simulations in large ECS architectures where many other systems are involved.

Acknowledgements

This project has received funding from the Clean Sky 2 Joint Undertaking (JU) under grant agreement No 886533. The JU receives support from the European Union's Horizon 2020 research and innovation programme and the Clean Sky 2 JU members other than the Union.



Carles Oliet, as a Serra Húnter Associate Professor, acknowledges the Catalan Government for the support through this Programme.

Disclaimer: The contents presented in this article reflect only the author's point of view: the authors and Clean Sky JU are not responsible for any use that may be made of the information it contains.

References

- Ablanque, Nicolás et al. (2023-08). "Vapour Compression Cycle Modelling for Use within Large Thermal Systems". In: *26th International Congress of Refrigeration (ICF2023)*. DOI: 10.18462/iir.icr.2023.0790.
- Acquaviva, Alessandro et al. (2020). "Analytical conduction loss calculation of a mosfet three-phase inverter accounting for the reverse conduction and the blanking time". In: *IEEE Transactions on Industrial Electronics* 68.8, pp. 6682–6691. DOI: 10.1109/TIE.2020.3003586.
- Bierhoff, Michael H and Friedrich W Fuchs (2004). "Semiconductor losses in voltage source and current source IGBT converters based on analytical derivation". In: *2004 IEEE 35th Annual Power Electronics Specialists Conference (IEEE Cat. No. 04CH37551)*. Vol. 4. IEEE, pp. 2836–2842. DOI: 10.1109/PESC.2004.1355283.
- Demiray, Turhan (2008). "Simulation of power system dynamics using dynamic phasor models". PhD thesis. ETH Zurich. URL: <https://doi.org/10.3929/ethz-a-005566449>.
- Gurumurthy, Sriram Karthik et al. (2022). "Hybrid Dynamic Phasor Modeling Approaches for Accurate Closed-Loop Simulation of Power Converters". In: *IEEE Access* 10, pp. 101643–101655. DOI: 10.1109/ACCESS.2022.3208963.
- Holmes, D Grahame and Thomas A Lipo (2003). *Pulse width modulation for power converters: principles and practice*. Vol. 18. John Wiley & Sons. URL: <https://ieeexplore.ieee.org/servlet/opac?bknumber=5264450>.
- Irwin, J David (1997). *The industrial electronics handbook*. CRC press.
- Krause, Paul C et al. (2013). *Analysis of electric machinery and drive systems*. Vol. 75. John Wiley & Sons. URL: <https://ieeexplore.ieee.org/servlet/opac?bknumber=5265638>.
- Loka, Nasrulloh Ratu Bagus Satrio et al. (2022). "Surrogate Modelling of Dynamic Phasor Simulations of Electrical Drives". In: *IECON 2022–48th Annual Conference of the IEEE Industrial Electronics Society*. IEEE, pp. 1–6. DOI: 10.1109/IECON49645.2022.9968552.
- Ruan, Xinbo et al. (2018). *Control techniques for LCL-type grid-connected inverters*. Springer. DOI: 10.1007/978-981-10-4277-5.
- Sarlioglu, Bulent and Casey T Morris (2015). "More electric aircraft: Review, challenges, and opportunities for commercial transport aircraft". In: *IEEE transactions on Transportation Electrification* 1.1, pp. 54–64. DOI: 10.1109/TTE.2015.2426499.